JACS
JOURNAL OF THE AMERICAN CHEMICAL SOCIETY
Article
pubs.acs.org/JACS

Controlling the Mechanism of Phase Transformation of Colloidal In_2O_3 Nanocrystals

Lisa N. Hutfluss and Pavle V. Radovanovic*

Department of Chemistry, University of Waterloo, 200 University Avenue West, Waterloo, Ontario N2L 3G1, Canada

Supporting Information

ABSTRACT: Controlling the crystal structure of transparent metal oxides is essential for tailoring the properties of these polymorphic materials to specific applications. The structural control is usually done via solid state phase transformation at high temperature or pressure. Here, we report the kinetic study of *in situ* phase transformation of In_2O_3 nanocrystals from metastable rhombohedral phase to stable cubic phase during their colloidal synthesis. By examining the phase content as a function of time using the model fitting approach, we identified two distinct coexisting mechanisms, surface and interface nucleation. It is shown that the mechanism of phase transformation can be controlled systematically through modulation of temperature and precursor to solvent ratio. The increase in both of these parameters leads to gradual change from surface to interface nucleation, which is associated with the increased probability of nanocrystal contact formation in the solution phase. The activation energy for surface nucleation is found to be 144 ± 30 kJ/mol, very similar to that for interface nucleation. Despite the comparable activation energy, interface nucleation dominates at higher temperatures due to increased nanocrystal interactions. The results of this work demonstrate enhanced control over polymorphic nanocrystal systems and contribute to further understanding of the kinetic processes at the nanoscale, including nucleation, crystallization, and biomineralization.

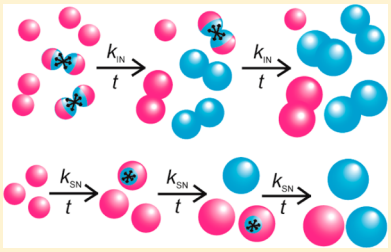

INTRODUCTION

The ability to tailor the size and phase of nanocrystals (NCs) is invaluable in the materials design process.[1−3] These parameters critically determine physical properties of materials, allowing for an expansion and manipulation of the available functionalities.[4−9] Isolation of a phase with distinctive properties can be achieved through understanding of the kinetics of phase stabilization and transformation.[10−15] Transparent metal oxides (TMOs) are of particular interest in this context because their transparency, conductivity, chemical stability, and polymorphism lend these materials to various applications including, but not limited to, electrodes, transistors, liquid crystal and touch screen displays, light emitting devices, and sensors.[16−21] The unequal accessibility of TMO polymorphs under ambient conditions poses an added challenge, making them ideal candidates for study motivated by both fundamental understanding of the phase transformation and the possibility of new applications.[22] Much work has been done on understanding the phase transformation of a variety of TMO nanocrystalline systems, including TiO_2,[15,23−25] ZnO,[26,27] V_2O_3,[28,29] and In_2O_3.[10,30−33] The focus of the current work is In_2O_3, which has two experimentally established crystal structures, namely, the stable cubic (bixbyite; bcc-In_2O_3) and metastable rhombohedral (corundum; rh-In_2O_3) phases.[34] Additionally, In_2O_3 has a wide band gap, ∼3.75 eV, and its transparency and possible high charge carrier mobility make it technologically important.[10,20,35,36] In addition to its technological appeal, the existence of only two phases makes In_2O_3 an ideal model system for phase transformation studies.

The specific surface energies and the inverse relationship between NC size and intrinsic surface stress are useful tools for controlling the structure at the nanoscale. Strongly reduced NC sizes result in high surface area to volume ratios and thus sufficient surface stress,[10,33,37−39] which could lead to stabilization of high energy crystal structures. Consequently, the formation of metastable phases is possible below certain NC size.[10,15,33] Knowing the critical size at which a phase transformation occurs allows for the preparation of nanomaterials with a well-defined phase via size control. Similarly, phase can be controlled through the application of pressure, which is a more traditional route employed for bulk materials[40,41] but has more recently been applied to nanoscale systems.[42,43] Temperature is also a critical factor in overcoming energy barriers to phase transformation in both bulk and nanomaterials,[40,44,45] and can be used to alter the mechanism by which the transformation occurs.

Many solid state models describing nucleation and growth have been developed, accounting for influential factors such as conversion fraction, temperature, and number of nucleation sites.[13,46−50] These models quantitatively and qualitatively describe reaction kinetics in solid state materials. Among them, the models based on the theoretical concepts developed by Avrami are most common and generally applicable to phase transformation processes.[50−52] The Johnson−Mehl−Avrami−Erofeev−Kolmogorov (JMAEK) model is distinguished by its

Received: September 12, 2014
Published: December 24, 2014

DOI: 10.1021/ja5094056
J. Am. Chem. Soc. 2015, 137, 1101−1108

consideration of nuclei ingestion and coalescence, as well as its ability to accurately determine the activation energy for a variety of systems, despite seemingly limiting assumptions made during derivation.[14,50,52] More recently developed by Zhang and Banfield, the surface and interface nucleation models were employed to describe the solid state phase transformation of anatase to rutile TiO_2 nanoparticles in powder form.[15,45,53] Interface nucleation (IN) involves the formation of a nucleation site at a particle−particle contact point, after which the new phase rapidly consumes the two particles. By contrast, surface nucleation (SN) relies on the formation of the nucleation sites on individual particle surfaces through random thermal fluctuations of atoms in order to initiate phase transformation. Additionally, these two mechanisms can simultaneously be at work, giving rise to a combined mechanism (IN+SN). The activation energies for IN and SN mechanisms often differ; in IN, interfacial defects such as lattice vacancies or dislocations generally result in lower energy barriers to the transformation to a more stable state. Temperature, particle size, and packing density of particles have been found to have a strong influence on the mechanism by which the transformation occurs and thus the activation energy required to complete the transformation.[15,45,53] While most of the reported kinetic studies focus on the phase transformation of TiO_2 nanopowder, much less is known about the mechanism of phase transformation occurring in solution during the synthesis of colloidal NCs. Such investigations are essential for achieving a thorough control of the structure and properties of this promising class of materials. Exploring the *in situ* phase transformation in solution also provides the opportunity to establish the correlation between NC growth and phase transformation, while eliminating the influence of substrate, nanoparticle spacers, aggregation, or other effects. Furthermore, to understand general principles governing the NC phase transformation in solution, the mechanistic studies have to be expanded to a broader range of materials, including other TMO NCs.

In this work, we report the comprehensive kinetic study of phase transformation of colloidal In_2O_3 NCs during their growth and demonstrate for the first time the ability to control *in situ* the mechanism of phase transformation in solution phase. It has previously been shown that In_2O_3 NCs undergo phase transformation from the metastable rhombohedral to stable cubic phase by the IN mechanism in colloidal suspension.[14] The activation energy for this process was determined to be ca. 150 kJ/mol under the given temperature and precursor concentration conditions. Here, we show that the phase transformation accompanying the solution phase synthesis of In_2O_3 NCs is indeed a more complex phenomenon. It is possible to vary the mechanisms of phase transformation between complete IN, SN, or a combination of the two through systematic manipulation of external parameters, including temperature, precursor to solvent ratio, and time. By doing so, we quantified the difference between the kinetic parameters of these two mechanisms and gained further insight into the fundamental processes involved in colloidal NC phase transformation that can lead to enhanced control and development of In_2O_3 and other TMO NC systems.

EXPERIMENTAL SECTION

Materials. All reagents and solvents were used as provided by the manufacturer without further purification. Indium acetylacetonate ($In(acac)_3$; 98%) was purchased from STREM Chemicals. Oleylamine (70%) and trioctylphosphine oxide (TOPO; 90%) were purchased from Sigma-Aldrich. Solvents utilized include toluene (EMD Chemicals; 99.98%) and absolute ethanol.

Methods. The In_2O_3 NC synthesis has been previously reported and was further modified for this study.[10,14] $In(acac)_3$ (6.11 mmol) and oleylamine (122 mmol) were combined in a 100 mL round-bottom flask to give a 1:20 molar ratio of precursor to solvent. In subsequent reaction sets, the amount of oleylamine was reduced to obtain 1:16 and 1:12 precursor to solvent molar ratios. The reflux system was assembled, and the mixture was degassed with stirring for 15 min. The mixture was then heated to the desired reaction temperature over the course of 1 h. Both the external and internal flask temperatures were recorded regularly throughout preheating and reaction time periods. The average internal flask temperature from the reaction start to finish was taken as the true temperature in further analysis.[54] For all reactions, we used the identical setup and the same equipment (flask, thermometer, and stirring bar). By sensitive adjustment of the heat settings and continuous temperature recording throughout the duration of the reaction, the temperature fluctuations were limited to ca. ±2.5 °C. Samples were extracted at designated times using a glass syringe, placed in a test tube and promptly sealed with parafilm. Once the final reaction time was reached, the sample was removed from heat and cooled naturally to room temperature while stirring under argon. The colloidal samples were precipitated with ethanol and isolated through centrifugation at 3000 rpm for 5 min. The supernatant liquid was discarded, and the washing process with ethanol was repeated two more times. A portion of the final samples was preserved in ethanol, while the majority of the material was dried and crushed into a fine powder. The precipitated samples held in ethanol were centrifuged, combined with an approximately equivalent volume of TOPO, and stirred in a 90 °C oil bath for 1 h. After the treatment was complete, the samples were precipitated and washed with ethanol. The TOPO treatment was repeated, if necessary, and the NC product was finally suspended in hexane to form clear colloidal suspensions.

Characterization of Phase Content. X-ray diffraction (XRD) patterns were collected with an INEL XRG 3000 powder X-ray diffractometer using Cu Kα radiation source (λ = 1.540598 Å), a germanium crystal monochromator, and an INEL CPS 120 curved position sensitive detector operating at 30 kV and 30 mA. Powder samples were loaded into an aluminum sample holder, and each pattern was collected for up to 2 h to obtain sufficiently high signal-to-noise ratio. The samples were prepared for TEM imaging by dispersing a small amount of precipitated fine powder in toluene, followed by extensive sonication and subsequent dilution. Samples were then deposited on copper grids with lacey Formvar/carbon support films purchased from Ted Pella, Inc. TEM images were collected using a JEOL-2010F microscope operating at 200 kV. X-ray absorption spectroscopy (XAS) measurements were completed at the 06ID-1 beamline at the Canadian Light Source (CLS) using liquid nitrogen-cooled double crystal monochromator, consisting of two crystal pairs (Si(111) and Si(220)). A Sn foil standard (K-edge at 29200 eV) was used for indium K-edge energy calibration. Spectra were recorded in transmission mode with three ionization chambers, the first two of which monitored the incident and transmitted X-ray intensities, respectively, while the third one was used as additional internal calibration for the In K-edge position.

Data Analysis. All XRD patterns were collected using the same instrument parameters and calibration, and were analyzed by linear combination and peak deconvolution upon the background subtraction. For both analyses, all patterns were baseline-corrected in the 2θ range 25−40° by spline interpolation. Linear combination of XRD patterns has been proven an effective method for the determination of phase content in this work.[14] XRD patterns of pure rh-In_2O_3, bcc-In_2O_3, and InOOH samples having different NC sizes synthesized at different temperatures by the method described above were used as reference materials in the linear combination analysis, where they were added in varied proportions to reproduce the experimental data. Considering that InOOH is a precursor to rh-In_2O_3, calculations involving the rh-In_2O_3 fraction included the InOOH content as well,[10] when this species was present. To account for an error introduced by linear combination analysis, the bcc-In_2O_3 fractional content (bcc content) was considered

DOI: 10.1021/ja5094056
J. Am. Chem. Soc. 2015, 137, 1101−1108

in terms of the maximum and minimum fraction of bcc-In_2O_3 that could reasonably fit the experimental patterns based on the overall difference between the experimental pattern and linear combination. The average composition was then taken as the true bcc content. For the deconvolution analysis, we used the same 2θ range as for linear combination. The phase contents of In_2O_3 NCs were calculated by fitting the overlapped bcc-In_2O_3 (222) and (400) and rh-In_2O_3 (104) and (110) peaks, allowing for variable broadening of the XRD peaks based on the average NC size.[14] The intensities of the peaks were set proportionally to their standard referenced intensities. The phase content was reported as an average value of the linear combination and peak deconvolution analysis, and the error bars are associated deviations from the average value. Fitting of models to experimental data was performed using the Trust Region algorithm. Extended X-ray absorption fine structure (EXAFS) data analysis was completed as described previously,[14] and the phase content at different times in the reaction was determined by a linear combination of pure phases as references.

RESULTS AND DISCUSSION

The kinetic investigations of phase transformation were performed by analyzing the change in the phase content during the synthesis of NCs using different precursor to solvent ratios. Unlike nanocrystalline powder, in colloidal suspensions, the size and concentration of NCs can be accurately and reproducibly controlled, which is essential for examination of the influence of these parameters on the phase transformation mechanism. Figure 1 shows the XRD patterns of the samples synthesized

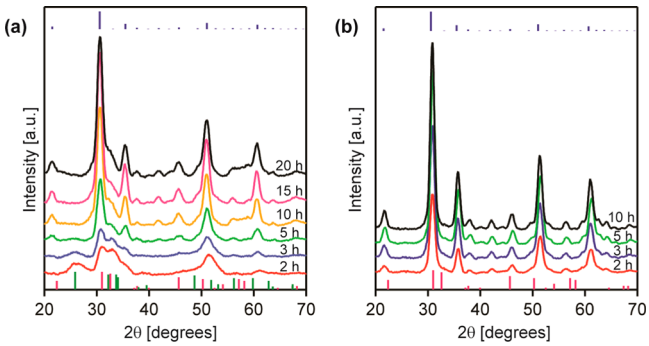

Figure 1. X-ray diffraction patterns of samples synthesized at (a) 200 and (b) 224 °C over the course of 20 h. Precursor to solvent ratio is 1:20. Blue sticks at the tops of the graphs indicate the bcc-In_2O_3 bulk pattern (JCPDS 06-0416), while pink and green sticks at the bottoms indicate rh-In_2O_3 (JCPDS 21-0406) and InOOH (JCPDS 17-0549) bulk patterns, respectively.

using 1:20 precursor to solvent ratio at 200 and 224 °C. For the 200 °C reaction temperature (Figure 1a), at short times the sample consists of a mixture of rh-In_2O_3 and InOOH with small amounts of bcc-In_2O_3. At longer times, the phase content becomes a mixture of rh-In_2O_3 and bcc-In_2O_3 only, as InOOH undergoes dehydration to form rh-In_2O_3 NCs prior to transformation to the cubic phase. The presence of InOOH and its subsequent disappearance at an early stage of the synthesis is consistent with the cascade dehydration mechanism of In_2O_3 NC formation previously reported (Figure S1 in Supporting Information).[10,36] The peaks corresponding to rh-In_2O_3 and InOOH are significantly broader than those corresponding to bcc-In_2O_3, suggesting that phase transformation from rh- to bcc-In_2O_3 accompanies NC growth. At higher temperature (Figure 1b), the samples display largely bcc-In_2O_3 phase even at short times, with no InOOH present, indicating faster particle formation and phase transformation with increasing temperature.

Determination of the bcc-In_2O_3 fractional content through linear combination is demonstrated in Figure 2a (bottom) for a

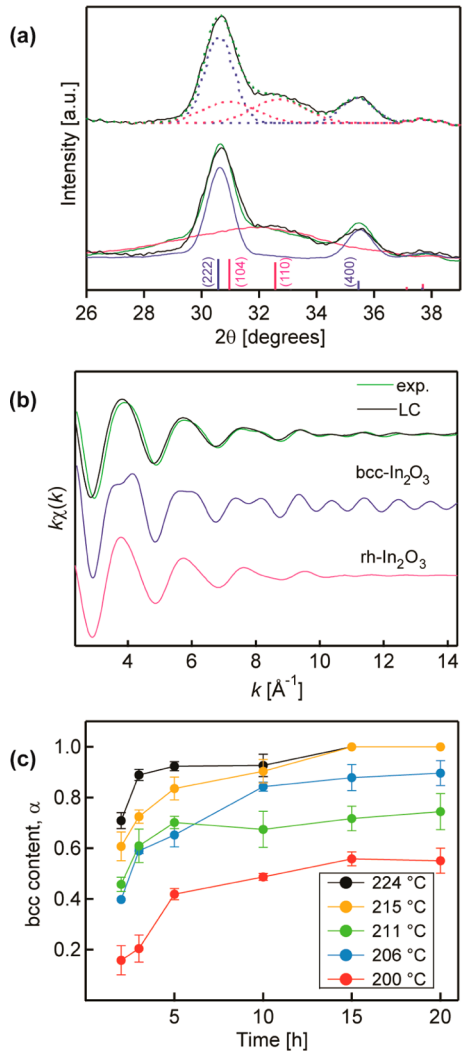

Figure 2. (a) Experimental XRD pattern (black lines) and the linear combination (bottom) and peak deconvolution (top) analysis for a 5 h sample from the 1:20 precursor to solvent series at 200 °C. Experimental XRD patterns of reference rh-In_2O_3 and bcc-In_2O_3 NCs for linear combination analysis are shown in pink and blue, respectively, and the resulting linear combination pattern is shown in green. The same colors but dashed lines are used for showing the deconvolution analysis. Bulk reference patterns for rh-In_2O_3 and bcc-In_2O_3 are shown by pink and blue sticks, respectively. (b) Linear combination (black) of rh-In_2O_3 (pink) and bcc-In_2O_3 (blue) EXAFS spectra to determine the phase content of a sample synthesized at 200 °C (green). (c) bcc-In_2O_3 fractional phase content as a function of time for samples synthesized using 1:20 precursor to solvent ratio at varying temperatures.

sample taken at 5 h from the 1:20 precursor to solvent series at 200 °C. The sharpness of the bcc-In_2O_3 (222) and (400) peaks relative to the broad (104) and (110) peaks of rh-In_2O_3 leads to significant changes in the linearly combined pattern with only relatively slight changes in the bcc phase content. The experimental XRD pattern (black line) is in excellent agreement with the pattern corresponding to 42% bcc phase and 58% rh phase (green line). These results were confirmed by the peak

DOI: 10.1021/ja5094056
J. Am. Chem. Soc. 2015, 137, 1101−1108

deconvolution method (Figure 2a, top).[14] A good agreement is obtained even in cases involving InOOH at the very early stage in the reaction (Figure S2 in Supporting Information). The average NC sizes necessary for reproducing the peak broadening generally match NC sizes corresponding to the reference patterns for the linear combination. The agreement between the phase content results obtained by deconvolution and linear combination methods is demonstrated in Table S1 (Supporting Information). To confirm the results of the XRD analysis, we used In K-edge EXAFS spectroscopy, which is sensitive to the local environment of In sites and can also serve as a quantitative measure of the phase content. Figure 2b shows a selected Fourier-filtered EXAFS spectrum of a sample prepared at 200 °C for somewhat later time into the reaction (green), together with the spectra of pure rh-In_2O_3 (pink) and bcc-In_2O_3 (blue) NCs as references. The linear combination analysis (black line) reveals ca. 20% bcc phase content, which is in good agreement with XRD analysis (15%). Figure 2c plots the bcc-In_2O_3 content of the 1:20 precursor to solvent series over time, illustrating that the conversion from rh-In_2O_3 to bcc-In_2O_3 is accelerated with increasing temperature, as anticipated. Under isothermal conditions, the rate of reaction decelerates with time at any given temperature. This observation applies to other dilution series, although the overall rate of phase transformation is strongly dependent on the solvent to precursor ratio (Figure S3 in Supporting Information). The bcc-In_2O_3 content, α, can then be utilized in kinetic modeling of the phase transformation process according to previously developed models.[14,45] In derivation of the kinetic models of phase transformation, it has been found that the equations for different models could be rearranged such that the left-hand side is common to all expressions, and this portion was subsequently denoted as y (eq 1).

$$y = \frac{(D_{rh}/D_o)^3}{(1-\alpha)} - 1 \tag{1}$$

Here, D_{rh} represents the average rhombohedral NC size at a given time and D_o the initial average rhombohedral NC size, which is taken to be the rh-In_2O_3 NC size at the earliest time point in the reaction. The D_o and D_{rh} were obtained from the peak broadening in the deconvolution analysis and confirmed using TEM images of the corresponding NC population at a given point in time. The D_o values range between 2.0 and 3.5 nm, depending on reaction temperature.

Equation 1 is employed to obtain the experimental y values for each sample at different points in time during the synthesis. Using the ability to control NC interactions in solution phase by varying the starting precursor concentrations, we applied this model-fitting approach to examine the experimental data in the context of different mechanisms involving NC surfaces, particularly SN and IN.[45] This analysis allows for identification of the underlying phase transformation mechanism and determination of the associated parameters through fitting of the y data with different models. We focused here on the surface-based mechanisms owing to the importance of high-energy sites in promoting the nucleation of a new phase. Equations 2 and 3 are used to model IN and SN mechanisms, respectively,

$$y(\mathrm{IN}) = k_{IN}N_o t_x(1 - e^{-t/t_x}) \tag{2}$$

$$y(\mathrm{SN}) = e^{k_{SN}t} - 1 \tag{3}$$

where t is time in both models and k_{IN} and k_{SN} are the interface and surface nucleation rate constants, respectively. In eq 2, N_o is the initial number of rhombohedral particles (often shown combined with k_{IN}), and t_x is the time at which the IN mechanism no longer contributes to phase transformation and the function levels off. The coexistence of IN and SN mechanisms can be represented simply by the sum of eqs 2 and 3, as an approximation for the combined mechanism.[45] In particular, the sum of eqs 2 and 3 was utilized in the TiO_2 phase transformation study, in which Al_2O_3 particles served as a spacer between TiO_2 particles, mimicking the dilute conditions in the nanopowder form.[45] The short-time linear and long-time exponential behavior of experimental data is indicative of IN dominance at short times and SN dominance at long times in the combined model. The combined SN and IN mechanism of phase transformation can also be described by the derived kinetic equation.[45]

$$y(\mathrm{IN} + \mathrm{SN}) = \left(1 + \frac{k_{IN}N_o}{k_{SN}}\right)(e^{k_{SN}t} - 1) \tag{4}$$

This expression is shown to accurately fit the experimental data involving both mechanisms under ideal conditions. When the IN contribution diminishes, $k_{IN}N_o$ approaches zero, and the remaining equation describes the SN mechanism alone (eq 3). Furthermore, for either very long or very short times, eq 2 can be reduced to $y(\mathrm{IN}) = k_{IN}N_o t$, which is the ideal form of the IN mechanism.[14,45]

The y values for samples of the 1:20 series synthesized at different temperatures are plotted as a function of time in Figure 3, together with the best fitting model for each temperature set, identified based on adjusted coefficient of determination (R-squared, R^2) values and visual inspection. Figure 3a shows the y values for the lowest temperature in the series (200 °C); further decrease in the reaction temperature under the given conditions results in incomplete conversion of InOOH to rh-In_2O_3, and no phase transformation to bcc-In_2O_3 (Figure S1 in Supporting Information). The data in Figure 3a is best fit with eq 3.[55] With increasing temperature, the most appropriate model to describe phase transformation shifts systematically from SN to IN. The y data in Figure 3b is fit in two portions; data ranging from the starting point at 2 to 10 h were best fit with eq 2, while data ranging from 10 to 20 h were best fit with eq 3. With further increase in the reaction temperature (224 °C), the best fit is achieved with eq 2, indicating the dominant contribution from the IN mechanism (Figure 3c). This can be understood in the context of the NC contact probability, where higher temperatures lead to larger available kinetic energy and thus increased chances of NC collisions within the dilute suspension, favoring the IN mechanism (*vide infra*). It should also be noted that fits were performed with an additional free parameter in the equations. This was done simply to prevent the function from being forced through the origin since these experimental data start at 2 rather than 0 h, which was the case in previous studies.[14,45] This delay is inherent to *in situ* phase transformation during colloidal synthesis in this work, as opposed to that of a preformed nanopowder phase.

In addition to the 1:20 precursor to solvent ratio, samples were also synthesized with a 1:16 and a 1:12 ratio in order to directly compare the dilute and concentrated NC suspensions. The most notable difference between the two extreme series is the rate of phase transformation; while the 1:20 ratio 200 °C series required 20 h to reach 60% conversion, the 1:12 series at nearly identical

DOI: 10.1021/ja5094056
J. Am. Chem. Soc. 2015, 137, 1101−1108

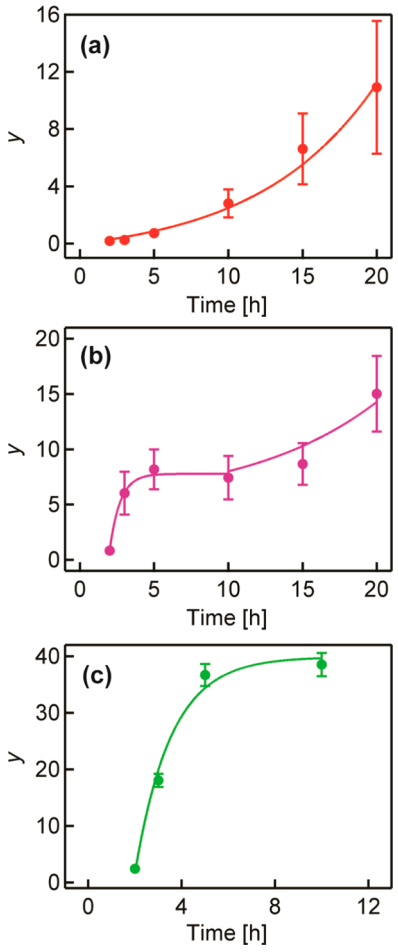

Figure 3. Kinetic data for phase transformation in samples synthesized with precursor to solvent ratio 1:20 at (a) 200, (b) 211, and (c) 224 °C. The solid lines are best fits to (a) y(SN), (b) y(IN)+y(SN), and (c) y(IN) models.

temperature (202 °C) reached 79% conversion after only 6 h (Figure S3 in Supporting Information). Additionally, the 1:20 series at 200 °C is a clear example of the SN mechanism, as evidenced by the fit with eq 3, whereas the 1:12 series at 202 °C is best modeled by the IN mechanism (Figure S4 in Supporting Information). This indicates that reduced particle contact probability in more dilute suspensions forces phase transformation to take place via the SN mechanism, which occurs at a significantly slower rate than the IN mechanism at the same temperature. These results demonstrate that it is possible to tune the mechanism and the degree of the phase conversion in the process of colloidal NC synthesis based on the precursor to solvent ratio and reaction temperature. By controlling these parameters, we were able to completely separate SN and IN mechanisms and achieve quantitative phase transformation by both mechanisms.

The kinetic parameters obtained from fitting with the most appropriate models are summarized in Table 1 for all dilution series.[14,45] The rate constants generally increase with increasing temperature for both SN and IN. At low precursor concentration, the reaction is dominated by SN, and the contribution from IN is observed only at high reaction temperatures. The combined IN and SN behavior is also observed in the y vs t curves for intermediate dilution (1:16) reactions, but at lower temperatures (196 and 203 °C). The IN contribution appears minor but not necessarily negligible early on in the reaction, with the remainder being dominated by the exponential SN behavior.

Table 1. Mechanisms of Phase Transformation and Kinetic Parameters for Sample Series of Varying Dilutions and Temperatures

dilution	T	model	k_{SN} [h^{-1}]	$k_{IN}N_o$ [h^{-1}]
1:20	200	y(SN)	0.1251	
	206	y(SN)	0.2145	
	215	y(IN+SN)	0.3359	1.086
	224	y(IN)		23.58
1:16	196	y(SN)	0.1410	
		y(IN+SN)	0.1327	0.0212
	203	y(SN)	0.2421	
		y(IN+SN)	0.2134	0.7044
	215	y(IN)		2.60
1:12	202	y(IN)		5.297
	212	y(IN)		10.29

Comparing the fits employed for different temperatures for a given dilution series, in particular the 1:20 series, reveals the systematic change in mechanism from SN to IN with increasing temperature and constant precursor to solvent ratio. This change illustrates that temperature provides another convenient avenue through which the mechanism can be controlled. These trends are summarized pictorially in Figure 4, which maps the dominant phase transformation mechanism observed for each dilution series (indicated with corresponding colors) at different temperatures. As either temperature or precursor to solvent ratio is increased, the mechanism of phase transformation shifts from SN to IN, eventually becoming entirely IN. It should be noted that the phase transformation occurs in a surprisingly narrow temperature range, allowing for the acquisition of a relatively limited number of data points to model the phase transformation mechanisms. The results of this work thus suggest that through simultaneous control of temperature and precursor to solvent ratio, the mechanism of the nucleation of a new phase in the phase transformation process can be controlled in a colloidal NC system.

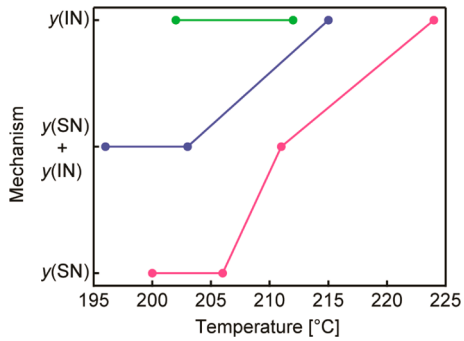

Figure 4. Mechanistic map showing the change in the mechanism of phase transformation through temperature and precursor to solvent ratio. Pink, blue, and green markers represent 1:20, 1:16, and 1:12 precursor to solvent ratios, respectively. Lines serve as a guide to the eye.

Figure 5 shows the Arrhenius plot constructed using the k_{SN} values from the 1:20 dilution series obtained at different temperatures. Using the Arrhenius expression (eq 5), these data were fitted, and the activation energy, E_a, and pre-exponential factor, A_o, were extracted.

DOI: 10.1021/ja5094056
J. Am. Chem. Soc. 2015, 137, 1101−1108

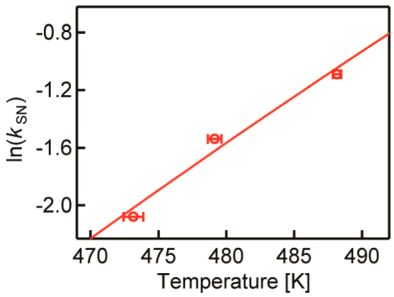

Figure 5. Arrhenius plot using the data for the most dilute series (1:20 precursor to solvent ratio). Solid line is the best fit to data points using eq 5.

$$\ln(k) = \ln(A_o) - \frac{E_a}{RT} \quad (5)$$

The activation energy for the SN process, E_a(SN), was determined to be ca. 124 kJ/mol, and A_o(SN) is 7.0×10^{12} h^{-1}.[56] The same analysis was performed for other dilutions (Figure S5 in Supporting Information), and the average E_a for SN was calculated to be 144 ± 30 kJ/mol. This is an interesting and somewhat surprising result, since SN is expected to be a higher energy process than IN for which E_a(IN) was determined to be ca. 150 kJ/mol in the previous studies involving IN-driven phase transformation of colloidal In_2O_3 NCs[14] and also confirmed in this work. Similar values of the activation energies are consistent with a very narrow temperature range in which the phase transformation occurs for this system. Unlike SN, which requires thermal fluctuations of atoms on rh-In_2O_3 NC surfaces to initiate the nucleation of a new phase, IN relies on the formation of cubic-like structure at the subset of rh-In_2O_3 NC interfaces to initiate the nucleation of the bcc-In_2O_3 phase. Our results suggest that both processes may ultimately involve similar rearrangements of bonds. This is in contrast to anatase-to-rutile TiO_2 nanopowder phase transformation, for which E_a(SN) and E_a(IN) were found to be 466 and 167 kJ/mol, respectively.[14,45] These results indicate not only that it is possible to manipulate *in situ* the mechanism of phase transformation during the synthesis of colloidal metal oxide NCs, but that the nucleation of a new phase is largely governed by local bonding rearrangement initiated by high-energy surface sites, rather than macroscopic properties of materials. Although SN and IN have similar activation energy, increasing temperature favors IN, as discussed above (Figures 3 and 4). This interesting and seemingly counterintuitive relationship is also different from that for TiO_2 nanopowder phase transformation, for which SN is found to dominate at higher temperatures. In colloidal suspensions, the probability of NC collision is based on Brownian motion, which also increases with temperature. In the kinetically driven phase transformation in NC suspension, SN then may become a primary mechanism at lower temperature not only because of the lower E_a, but also by reducing the NC interactions. These results indicate that the phase transformation of NCs during the colloidal synthesis is determined by different principles than the transformation of NCs in the powder form.

To provide a supporting evidence for phase transformation mechanisms under different conditions, we employed TEM imaging and analysis. Overview TEM images of NCs synthesized at 200 °C using 1:20 precursor to solvent ratio, 5 h after the final reaction temperature had been reached, are shown in Figure S6, Supporting Information. Most NCs exhibit nearly spherical shape, although there are a few displaying elliptical or dumbbell morphology. Figure 6a shows a typical image of a single rh-In_2O_3 NC from this sample. The NC appears to have quasi-spherical or

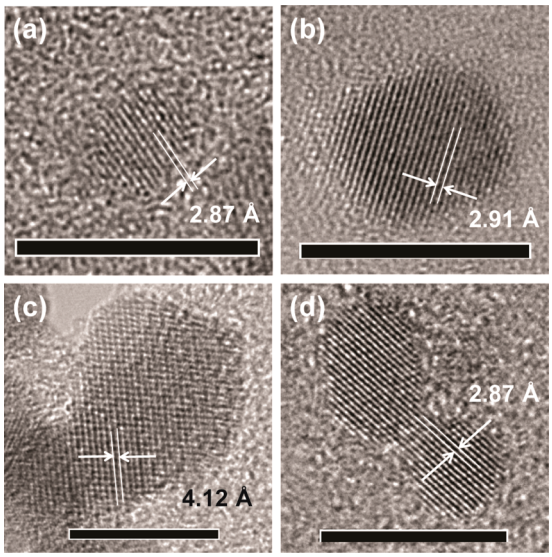

Figure 6. Typical lattice-resolved TEM images of individual NCs in the course of the colloidal synthesis. (a, b) NCs obtained after 5 h at 200 °C for 1:20 precursor to solvent ratio: (a) rh-In_2O_3 NC identified by the {104} plane and (b) bcc-In_2O_3 NC identified by the {222} plane, illustrating the possibility of phase transformation via SN mechanism. (c) NCs obtained after 2 h at 200 °C for 1:12 precursor to solvent ratio. NCs having bcc-In_2O_3 structure identified by the {211} plane are joined by oriented attachment, demonstrating that phase transformation also occurs by IN mechanism. (d) Oriented-attached rh-In_2O_3 NCs showing no phase transformation upon contact formation. Scale bars in all images, 10 nm.

rectangular shape, measuring ca. 4.3 nm in diagonal direction. The measured lattice spacing of 2.87 Å corresponds to the {104} lattice plane of rh-In_2O_3. The same sample contains both rh- and bcc-In_2O_3 phase, as evident from the corresponding XRD data in Figure 1. The critical NC size for phase transformation from rh- to bcc-In_2O_3 is ca. 5 nm.[10,14] Somewhat larger NCs with very similar morphology and lattice spacing of 2.91 Å corresponding to the {222} planes of bcc-In_2O_3 were also observed (Figure 6b), suggesting that phase transformation spontaneously occurs by SN once NCs attain the critical size. Although rh-In_2O_3 {104} and bcc-In_2O_3 {222} planes have similar lattice spacing, virtually all NCs smaller than the critical size exhibit an electron diffraction pattern characteristic for rh-In_2O_3.[10] Similar observations were made at shorter reaction times, consistent with the kinetic analysis in Figure 3a, indicating the dominant SN mechanism even early on in the reaction under these conditions (Figure S7, Supporting Information). However, increasing precursor to solvent ratio results in a dominant population of larger NCs that have irregular shapes derived by two joined NCs (Figures S8 and 9, Supporting Information). Figure 6c depicts two NCs joined via oriented attachment, with 4.12 Å lattice spacing also indicating bcc-In_2O_3 phase ({211} plane). This observation is consistent with the phase transformation initiated by IN at the particle−particle contact point. As expected, not all NC contact formation leads to the phase transformation. Figure 6d shows an example of two rh-In_2O_3 NCs joined by oriented attachment while retaining the corundum crystal structure. The interface between two NCs contains no observable dislocations or defects, which could form in oriented NC attachment[57] and

DOI: 10.1021/ja5094056
J. Am. Chem. Soc. 2015, 137, 1101−1108

are suggested to be necessary for phase transformation by IN.[58−60] The lack of interfacial defects is consistent with the retention of rh-In_2O_3 phase upon NC attachment. Importantly, all NCs examined by TEM consist only of a single phase. This observation is consistent with a very rapid single-step transformation once the new phase nucleates on the NC surfaces or interfaces. Taken together, the results of Figure 6 demonstrate that both IN and SN mechanisms will simultaneously play a role in phase transformation kinetics of colloidal NCs.

Overall, the results of this work are summarized pictorially in Figure 7. Figure 7a,b illustrates the effect of precursor

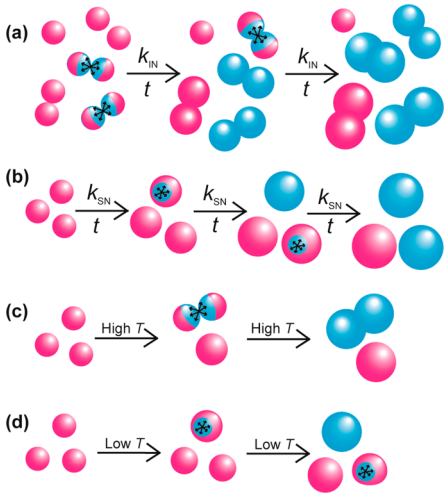

Figure 7. (a, b) Illustration of (a) IN and (b) SN phase transformation mechanisms through manipulation of the precursor to solvent ratio and allotted reaction time. (c, d) Illustration of temperature impact on the mechanism, where higher temperatures lead to IN (c) and lower temperatures allow for SN (d), respectively. Pink and blue spheres represent rh-In_2O_3 and bcc-In_2O_3 NCs, respectively.

concentration and reaction time on the phase transformation mechanism, using pink (rh-In_2O_3 NCs) and blue (bcc-In_2O_3 NCs) spheres. High NC concentration leads to high probability of contact formation and IN (Figure 7a), while SN is more likely to occur in diluted suspensions and requires longer times for the completion of phase transformation (Figure 7b). The formation of nucleation sites at NC contact points in IN is contrasted with the SN mechanism in which the nucleation site forms on the surface of a lone NC as it grows. Additionally, rh-In_2O_3 NCs can fuse by oriented attachment without undergoing phase transformation, if the joining NCs are sufficiently small and contain no defects or cubic-like motifs at the contact points, as depicted in Figure 7a. The role of the probability of NC contact formation for the mechanism of phase transformation is confirmed by comparing the reaction yield of the samples prepared using 1:12 and 1:20 precursor to solvent ratio at 200 °C, for the durations that result in similar NC sizes (Figure S10 in Supporting Information). The yield of the reaction for 1:12 dilution is ca. 25% higher than that for 1:20 sample, indicating overall significantly higher concentration of NCs for 1:12 sample. Furthermore, larger number of elongated (oblong or dumbbell-shaped) NCs is observed for 1:12 dilution sample, also consistent with IN mechanism. Figure 7c,d shows the impact of temperature on the phase transformation mechanism. Elevated temperatures lead to an enhancement in the rate of NC collisions and thus phase transformation by IN. At low temperatures, slower Brownian motion decreases the rate of NC contact formation and favors SN (Figure 7d). Understanding the influence of these variables allows for the control of the mechanism at work and the rate of the colloidal NC phase transformation process.

CONCLUSIONS

In summary, we investigated the kinetics of *in situ* phase transformation during the growth of colloidal In_2O_3 NCs. The coexistence of two distinct mechanisms of phase transformation were identified; the mechanism initiated by the nucleation of a new phase on the surface of individual NCs (SN), and at the interface between contacting NCs (IN). It is likely that high energy defect sites play an important role in enabling both mechanisms. We showed that through the control of temperature and precursor to solvent ratio, the mechanism of phase transformation can be controlled and systematically varied from pure SN to IN by increasing the aforementioned parameters. As a result, we mapped out the contribution of different mechanisms to the phase transformation occurring under different synthetic conditions. The two mechanisms are characterized by similar activation energy, ca. 150 kJ/mol. SN is found to be a predominant mechanism at lower temperatures, which is opposite from the trend reported for the phase transformation of TiO_2 NCs in the powder form. We propose that the change from SN to IN with increasing temperature is at least partly associated with increasing NC interactions, arising from the Brownian motion. The complete phase transformation by SN at low temperatures can still be achieved kinetically over a longer time scale. Comparison with the TiO_2 nanopowder phase transformation results suggests that the activation energies are determined by local metal−oxygen bond rearrangement, rather than macroscopic properties of the polymorphic materials. It is plausible that other more complex mechanisms of phase transformation are also possible under certain conditions, which represents an interesting topic for future investigations. The results of this work have general applicability, opening the doors for the examination of other colloidal polymorphic systems and the possibility of tailoring the properties of such materials for specific applications via structural transformations.

ASSOCIATED CONTENT

Supporting Information

Additional XRD patterns of samples isolated in the synthesis with 1:20 precursor to solvent ratio, proposed mechanism of In_2O_3 NC formation, additional kinetic data and analysis, additional TEM images for different dilutions and synthesis duration. This material is available free of charge via the Internet at http://pubs.acs.org.

AUTHOR INFORMATION

Corresponding Author

*pavler@uwaterloo.ca

Notes

The authors declare no competing financial interest.

ACKNOWLEDGMENTS

This work was supported by the Natural Sciences and Engineering Research Council of Canada (Discovery Grant) and Canada Research Chairs program (award to P.V.R.). TEM measurements were performed at the Canadian Centre for Electron Microscopy (Brockhouse Institute for Materials Research) at McMaster University. X-ray absorption spectros-

DOI: 10.1021/ja5094056
J. Am. Chem. Soc. 2015, 137, 1101−1108

copy measurements were performed at the Canadian Light Source, which is supported by the NSERC, NRC, CIHR, the Province of Saskatchewan, Western Economic Diversification Canada, and the University of Saskatchewan. We thank Natalie Sisombath for her aid in synthesis and XRD pattern collection.

REFERENCES

(1) Chen, C.-C.; Herhold, A. B.; Johnson, C. S.; Alivisatos, A. P. *Science* **1997**, *276*, 398−401.
(2) El-Sayed, M. A. *Acc. Chem. Res.* **2004**, *37*, 326−333.
(3) Kim, J. Y.; Voznyy, O.; Zhitomirsky, D.; Sargent, E. H. *Adv. Mater.* **2013**, *25*, 4986−5010.
(4) Bardhan, R.; Hedges, L. O.; Pint, C. L.; Javey, A.; Whitelam, S.; Urban, J. J. *Nat. Mater.* **2013**, *12*, 905−912.
(5) Zhang, S.; Zhang, X.; Jiang, G.; Zhu, H.; Guo, S.; Su, D.; Lu, G.; Sun, S. *J. Am. Chem. Soc.* **2014**, *136*, 7734−7739.
(6) Kuo, H.-H.; Chen, L.; Ji, Y.; Liu, H.-J.; Chen, L.-Q.; Chu, Y.-H. *Nano Lett.* **2014**, *14*, 3314−3320.
(7) Wang, T.; Radovanovic, P. V. *J. Phys. Chem. C* **2011**, *115*, 406−413.
(8) Farvid, S. S.; Hegde, M.; Radovanovic, P. V. *Chem. Mater.* **2013**, *25*, 233−244.
(9) Smith, M. B.; Page, K.; Siegrist, T.; Redmond, P. L.; Walter, E. C.; Seshadri, R.; Brus, L. E.; Steigerwald, M. L. *J. Am. Chem. Soc.* **2008**, *130*, 6955−6963.
(10) Farvid, S. S.; Dave, N.; Radovanovic, P. V. *Chem. Mater.* **2010**, *22*, 9−11.
(11) Aastuen, D. J. W.; Clark, N. A.; Cotter, L. K. *Phys. Rev. Lett.* **1986**, *57*, 1733−1736.
(12) Oxtoby, D. W. *Acc. Chem. Res.* **1998**, *31*, 91−97.
(13) Raju, S.; Mohandas, E. *J. Chem. Sci.* **2010**, *122*, 83−89.
(14) Farvid, S. S.; Radovanovic, P. V. *J. Am. Chem. Soc.* **2012**, *134*, 7015−7024.
(15) Zhang, H.; Banfield, J. F. *J. Mater. Chem.* **1998**, *8*, 2073−2076.
(16) Robertson, J.; Gillen, R.; Clark, S. J. *Thin Solid Films* **2012**, *520*, 3714−3720.
(17) Radovanovic, P. V. In *Functional Metal Oxides*; Ogale, S. B., Venkatesan, T. V., Blamire, M. G., Eds.; Wiley-VCH Verlag GmbH & Co.: Weinheim, Germany, 2013.
(18) Fortunato, E.; Ginley, D.; Hosono, H.; Paine, D. C. *MRS Bull.* **2007**, *32*, 242−247.
(19) Wan, Q.; Dattoli, E. N.; Fung, W. Y.; Guo, W.; Chen, Y.; Pan, X.; Lu, W. *Nano Lett.* **2006**, *6*, 2909−2915.
(20) O'Dwyer, C.; Szachowicz, M.; Visimberga, G.; Lavayen, V.; Newcomb, S. B.; Torres, C. M. S. *Nat. Nanotechnol.* **2009**, *4*, 239−244.
(21) Wang, T.; Chirmanov, V.; Chiu, W. H. M.; Radovanovic, P. V. *J. Am. Chem. Soc.* **2013**, *135*, 14520−14523.
(22) Sun, C.; Xue, D. *Curr. Opin. Chem. Eng.* **2012**, *1*, 108−116.
(23) Zheng, P.; Hao, R.; Zhao, J.; Jia, S.; Cao, B.; Zhu, Z. *J. Mater. Chem. A* **2014**, *2*, 4907−4911.
(24) Prasad, K.; Pinjari, D. V.; Pandit, A. B.; Mhaske, S. T. *Ultrason. Sonochem.* **2010**, *17*, 409−415.
(25) Azizi, K. F.; Bagheri-Mohagheghi, M.-M. *J. Sol-Gel Sci. Technol.* **2013**, *65*, 329−335.
(26) Lu, Q.; Yun, G.; Zhou, W.; Li, J. *J. Mater. Sci. Technol.* **2013**, *29*, 841−845.
(27) Solozhenko, V. L.; Kurakevych, O. O.; Sokolov, P. S.; Baranov, A. N. *J. Phys. Chem. A* **2011**, *115*, 4354−4358.
(28) Hong, W.-K.; Park, J. B.; Yoon, J.; Kim, B.-J.; Sohn, J. I.; Lee, Y. B.; Bae, T.-S.; Chang, S.-J.; Huh, Y. S.; Son, B.; Stach, E. A.; Lee, T.; Welland, M. E. *Nano Lett.* **2013**, *13*, 1822−1828.
(29) Bergerud, A.; Buonsanti, R.; Jordan-Sweet, J. L.; Milliron, D. J. *Chem. Mater.* **2013**, *25*, 3172−3179.
(30) Epifani, M.; Siciliano, P.; Gurlo, A.; Barsan, N.; Weimar, U. *J. Am. Chem. Soc.* **2004**, *126*, 4078−4079.
(31) Lee, C. H.; Kim, M.; Kim, T.; Kim, A.; Paek, J.; Lee, J. W.; Choi, S.-Y.; Kim, K.; Park, J.-B.; Lee, K. *J. Am. Chem. Soc.* **2006**, *128*, 9326−9327.
(32) Gurlo, A. *Angew. Chem., Int. Ed.* **2010**, *49*, 5610−5612.
(33) Farvid, S. S.; Dave, N.; Wang, T.; Radovanovic, P. V. *J. Phys. Chem. C* **2009**, *113*, 15928−15933.
(34) Gurlo, A.; Kroll, P.; Riedel, R. *Chem.—Eur. J.* **2008**, *14*, 3306−3310.
(35) Hamberg, I.; Granqvist, C. G. *J. Appl. Phys.* **1986**, *60*, R123−R159.
(36) Zhuang, Z.; Peng, Q.; Liu, J.; Wang, X.; Li, Y. *Inorg. Chem.* **2007**, *46*, 5179−5187.
(37) Jiang, Q.; Liang, L. H.; Zhao, D. S. *J. Phys. Chem. B* **2001**, *105*, 6275−6277.
(38) Vlasov, N. M.; Dragunov, Y. G. *Tech. Phys.* **2013**, *58*, 218−222.
(39) Zatryb, G.; Podhorodecki, A.; Misiewicz, J.; Cardin, J.; Gourbilleau, F. *Nanoscale Res. Lett.* **2013**, *8*, 40−46.
(40) Shannon, R. D. *Solid State Commun.* **1966**, *4*, 629−630.
(41) Chandra Shekar, N. V.; Govinda Rajan, K. *Bull. Mater. Sci.* **2001**, *24*, 1−21.
(42) Gupta, D. C.; Rana, P. *J. Mol. Model* **2012**, *18*, 3341−3350.
(43) Wu, H.; Wang, Z.; Fan, H. *J. Am. Chem. Soc.* **2014**, *136*, 7634−7636.
(44) Fontaine, D. D.; Paton, N. E.; Williams, J. C. *Acta Metall.* **1971**, *19*, 1153−1162.
(45) Zhang, H.; Banfield, J. F. *J. Mater. Res.* **2000**, *15*, 437−448.
(46) Embden, J. v.; Sader, J. E.; Davidson, M.; Mulvaney, P. *J. Phys. Chem. C* **2009**, *113*, 16342−16355.
(47) Malek, J.; Mitsuhashi, T.; Criado, J. M. *J. Mater. Res.* **2001**, *16*, 1862−1871.
(48) Villa, E.; Rios, P. R. *Acta Mater.* **2010**, *58*, 2752−2768.
(49) Vyazovkin, S.; Wight, C. A. *Annu. Rev. Phys. Chem.* **1997**, *48*, 125−149.
(50) Khawam, A.; Flanagan, D. R. *J. Phys. Chem. B* **2006**, *110*, 17315−17328.
(51) Avrami, M. *J. Chem. Phys.* **1939**, *7*, 1103−1112.
(52) Fanfoni, M.; Tomellini, M. *Nuovo Cimento Soc. Ital. Fis., D* **1998**, *20*, 1171−1182.
(53) Zhang, H.; Banfield, J. F. *Chem. Mater.* **2005**, *17*, 3421−3425.
(54) It should be noted for comparison purposes that our previous work involving IN mechanism (see refs 10 and 14) reported external rather than internal flask temperature, which was on average ca. 50 °C higher.
(55) When fit with eq 4 (combined model), the obtained SN rate constant, k_{SN}, is nearly identical to that obtained from fitting with eq 3, while the IN term, $k_{IN}N_o$, is nearly zero. This reinforces the identification of SN as the dominant mechanism of phase transformation in this case.
(56) As a check, the rearranged Arrhenius equation (eq S1 in Supporting Information), was utilized to estimate the activation energy using only two data points (see ref 45). In the case of the 1:20 dilution series, pairwise analysis using k_{SN} values and corresponding temperatures was completed using eq S1, the average of these results proving consistent with the full fitting. In the case of the 1:12 dilution series, E_a(IN) was calculated to be ca. 150 kJ/mol using eq S1, also illustrating consistency in the results.
(57) Penn, R. L.; Banfield, J. F. *Science* **1998**, *281*, 969−971.
(58) Shannon, R. D.; Pask, J. A. *J. Am. Ceram. Soc.* **1965**, *48*, 391−398.
(59) Kumar, K.-N. P.; Keizer, K.; Burggraaf, A. J. *J. Mater. Chem.* **1993**, *3*, 1141−1149.
(60) Iida, Y.; Ozaki, S. *J. Am. Ceram. Soc.* **1961**, *44*, 120−127.

DOI: 10.1021/ja5094056
J. Am. Chem. Soc. 2015, 137, 1101−1108